IIA^{Glc} Inhibition of Glycerol Kinase: A Communications Network Tunes Protein Motions at the Allosteric Site†

Peng Yu,‡ Mauricio Lasagna, Aaron C. Pawlyk,§ Gregory D. Reinhart, and Donald W. Pettigrew*

Department of Biochemistry and Biophysics and Texas Agricultural Experiment Station, Texas A&M University, College Station, Texas 77843-2128

Received June 4, 2007; Revised Manuscript Received August 24, 2007

ABSTRACT: Steady-state and time-resolved fluorescence anisotropy methods applied to an extrinsic fluorophore that is conjugated to non-native cysteine residues demonstrate that amino acids in an allosteric communication network within a protein subunit tune protein backbone motions at a distal site to enable allosteric binding and inhibition. The unphosphorylated form of the phosphocarrier protein IIA^{Glc} is an allosteric inhibitor of *Escherichia coli* glycerol kinase, binding more than 25 Å from the kinase active site. Crystal structures that showed a ligand-dependent conformational change and large temperature factors for the IIA^{Glc}-binding site on *E. coli* glycerol kinase suggest that motions of the allosteric site have an important role in the inhibition. Three *E. coli* glycerol kinase amino acids that are located at least 15 Å from the active site and the allosteric site were shown previously to be necessary for transplanting IIA^{Glc} inhibition into the nonallosteric glycerol kinase from *Haemophilus influenzae*. These three amino acids are termed the coupling locus. The apparent allosteric site motions and the requirement for the distant coupling locus to transplant allosteric inhibition suggest that the coupling locus modulates the motions of the IIA^{Glc}-binding site. To evaluate this possibility, variants of *E. coli* glycerol kinase and the chimeric, allosteric *H. influenzae* glycerol kinase were constructed with a non-native cysteine residue replacing one of the native residues in the IIA^{Glc}-binding site. The extrinsic fluorophore Oregon Green 488 (2′,7′-difluorofluorescein) was conjugated specifically to the non-native cysteine residue. Steady-state and time-resolved fluorescence anisotropy measurements show that the motions of the fluorophore reflect backbone motions of the IIA^{Glc}-binding site and these motions are modulated by the amino acids at the coupling locus.

Emerging views of allosteric control of protein functions extend and refine elements of the classical view (*1*−*3*). Allosteric behavior is not restricted to oligomeric proteins but may occur also between different ligand-binding sites of monomeric proteins. In the rugged landscape view of protein structure that has emerged from protein folding, biophysical, and computational studies, the unliganded protein samples many conformations in the absence of ligands. Within this ensemble of unliganded structures are conformations with higher affinity for ligand binding to one of the two sites, and ligand binding captures these conformations. When the captured conformations have different affinities for ligand binding or different catalytic properties at the second site, allosteric behavior is observed. These aspects of allostery were considered by Weber 35 years ago (*4*). Communication between the different ligand-binding sites involves not conformational changes that reflect global cooperativity but changes in local interactions among a few amino acid residues. These amino acids form networks for communication between the ligand-binding sites. The independence of heterotropic communication networks, i.e., absence of global cooperativity, has been demonstrated for oligomeric allosteric enzymes (*5*, *6*).

Within the context of the ensemble view of protein structure, protein motions that occur over a broad range of time scales may have roles in allosteric behavior (*2*, *7*, *8*). Time-resolved intrinsic tryptophan fluorescence anisotropy showed that internal motions of protein and protein−ligand species may be the basis for entropic contributions to allosteric effects (*9*). The recent reviews of the literature report examples for which ligand binding at one site alters the protein dynamics at a distal site (*10*−*12*). Here, we report

† Supported by Grants GM068768 (D.W.P.) and GM033216 (G.D.R.) from the National Institutes of Health and A-1479 (D.W.P.) and A-1543 (G.D.R.) from the Robert A. Welch Foundation and by the Texas Agricultural Experiment Station (Grant H-9208).

* To whom correspondence should be addressed. Phone: (979) 845-9621. Fax: (979) 845-9274. E-mail: dpettigrew@tamu.edu.

‡ Current address: Division of Translational Research, Department of Internal Medicine, University of Texas Southwestern Medical Center, 5323 Harry Hines Blvd., Dallas, TX 75390-9185.

§ Current address: Women's Health and Musculoskeletal Biology, Wyeth Research, 500 Arcola Rd., Collegeville, PA 19426.

[1] Abbreviations: IIA^{Glc}, the glucose-specific phosphocarrier protein of the phosphoenolpyruvate:glycose phosphotransferase system (TC 4.A.1); EcGK, *Escherichia coli* glycerol kinase; FBP, fructose 1,6-bisphosphate; G3P, L-glycerol 3-phosphate; GK, glycerol kinase (EC 2.7.1.30, ATP:glycerol 3-phosphotransferase); gol, glycerol; HiGK, *Haemophilus influenzae* glycerol kinase; homo-FRET, homo-Förster resonance energy transfer; IAF, (iodoacetamido)fluorescein; IAOG, iodoacetamido-OG; ns, nanosecond; OG, Oregon Green 488 (2′,7′-difluorofluorescein); PTS, phosphoenolpyruvate:glycose phosphotransferase system; TEA, triethanolamine; TRFA, time-resolved fluorescence anisotropy.

10.1021/bi7010948 CCC: $37.00
Published on Web 10/09/2007

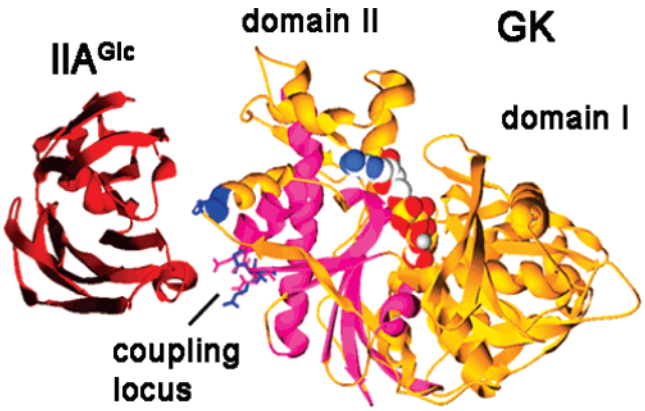

FIGURE 1: Structure of the IIA^{Glc}−EcGK complex. A ribbon diagram of the structure from PDB file 1GLC is shown for the complex of IIA^{Glc} bound to one subunit of EcGK. IIA^{Glc} is shown in red. EcGK is shown in gold with the conserved ATPase catalytic core elements of domain II shown in magenta. Active site ligands ADP and G3P of the kinase that are bound between domains I and II are shown as space-filling models. The regions that are transplanted from the EcGK to generate IIA^{Glc} inhibition in the HiGK^{II}L chimeric enzyme are shown in blue. The three amino acid residues that comprise the coupling locus are shown as sticks; EcGK residues are shown in blue, and HiGK residues are shown in magenta. The HiGK residue positions were obtained by modeling the HiGK structure by using the SWISS MODEL with PDB files 1GLA and 1GLC (*43*).

that amino acid changes that are required for evolution of a communication network to enable allosteric control of catalytic activity modulate the ns[1] dynamics of the distant allosteric ligand-binding site.

Allosteric inhibition of EcGK by IIA^{Glc} is an example of control of catalytic activity by protein−protein interactions in a signal transduction pathway. In its phosphocarrier role for glucose uptake by the PTS, IIA^{Glc} oscillates between being unphosphorylated and being phosphorylated at its active site histidine 90 (*13*, *14*). During glucose uptake, about 95% of the IIA^{Glc} is unphosphorylated, but it becomes highly phosphorylated when extracellular glucose is not available (*15*). EcGK, which catalyzes the initial step of glycerol utilization, is inhibited in vitro by the unphosphorylated form of the phosphocarrier protein IIA^{Glc}. The unphosphorylated form of IIA^{Glc} thus signals glucose availability to the pathway for glycerol utilization. It provides the same signal to pathways for utilization of other carbon sources including lactose, maltose, and melibiose, interacting with the respective transport system to prevent entry.

X-ray crystallographic studies provide important insights into IIA^{Glc} allosteric inhibition of EcGK. Crystal structures of EcGK show it is a member of the sugar kinase (FGGY kinase family)/actin/heat shock protein 70 superfamily (*16*, *17*). These enzymes are characterized by an active site cleft that is formed between two domains, which are termed domain I and domain II, as shown in Figure 1. Substrate binding to members of the sugar kinase superfamily is associated with closure of the active site cleft by movement of one domain relative to the other, as shown initially for hexokinase (*18*) and recently for rhamnulokinase (*19*). Crystal structures indicate a similar but smaller motion for binding of glycerol to the GK from *Enterococcus casseliflavus*, which shows 78% sequence similarity to EcGK (*20*). Relative domain motions about hinges calculated on the basis of different subunit conformations in crystals of EcGK variants support this characteristic conformational change for it (*21*, *22*). This conformational change has been characterized as an induced fit, and modulation of this motion is generally believed to be the basis for control of the catalytic activity of superfamily members (*20*, *23*).

The cocrystal structure of the EcGK−IIA^{Glc} complex shows that it is formed by binding of the active site region of IIA^{Glc} to domain II about 30 Å away from the GK active site (Figure 1) (*16*). The structure thus shows that phosphorylation of the active site histidine 90 residue eliminates inhibition of EcGK by sterically blocking complex formation. The IIA^{Glc}-binding site of EcGK consists of the amino acids at position 402 and the sequentially contiguous positions 472−481. Comparison of the cocrystal structure of the complex to that of EcGK alone shows a change in conformation of the sequentially contiguous region upon IIA^{Glc} binding (*24*). In the absence of IIA^{Glc}, this region is a coil for amino acids 472−475 and an α-helix for amino acids 476−481; this α-helix extends through residue 494. In the complex with IIA^{Glc}, this region is a 3_{10}-helix for amino acids 472−478 and an α-helix for amino acids 479−481. Comparison of the crystal structures of EcGK and the IIA^{Glc}-EcGK complex does not reveal how this conformational change at the IIA^{Glc}-binding site is related to the induced fit active site closure because the IIA^{Glc}-binding site conformational change is the only difference seen.

An approach that is based on construction of chimeric enzymes was used to investigate regions of EcGK that have roles in IIA^{Glc} allosteric control. A locus of three amino acids in EcGK that couples the IIA^{Glc}-binding site to inhibition of catalysis was identified by transplanting IIA^{Glc} inhibition into the GK from *H. influenzae* (*25*). The primary structure of HiGK is 87% similar/76% identical to that of EcGK, and HiGK is naive with respect to inhibition by *E. coli* IIA^{Glc} (*26*). The allosteric coupling region was identified by determining portions of EcGK that must be transplanted into HiGK to generate IIA^{Glc} inhibition of it. The residue at position 402 is arginine for both enzymes. The native amino acid sequence of the sequentially contiguous portion of the EcGK IIA^{Glc}-binding site is ...P_{472}GIETTE$_{478}$RNY$_{481}$..., and the corresponding sequence of HiGK is ...P_{472}DSDNEK$_{478}$-RER$_{481}$.... The chimeric enzyme HiGK^{II} was constructed by transplantation of the EcGK amino acid residues 473−481 into HiGK.[2] Although this chimeric enzyme contains all of the crystallographically identified IIA^{Glc}-binding site amino acid residues from EcGK, it is not inhibited by IIA^{Glc} and binding of IIA^{Glc} could not be detected. Additional transplantation of amino acid residues 427−429 from EcGK into HiGK^{II}, generating the chimeric enzyme HiGK^{II}L, is required to obtain allosteric inhibition by IIA^{Glc}. The reverse transplantation of amino acids 427−429 from HiGK into EcGK, generating the chimeric enzyme EcGKr, eliminates IIA^{Glc} allosteric control. The three amino acids at positions 427−429 are termed the coupling locus because they define a locus

[2] Nomenclature for glycerol kinase chimeric and variant enzymes: The superscript II indicates the sequentially contiguous amino acids 473−481 of the EcGK IIA^{Glc}-binding site, L indicates the amino acids 427−429 (GTR) from EcGK, and r indicates the amino acids 427−429 (DVN) from HiGK. Variant enzymes that contain a single nonnative cysteine residue are denoted by using single-letter amino acid abbreviations; e.g., I474C EcGK is the variant of EcGK in which isoleucine at position 474 is replaced by cysteine.

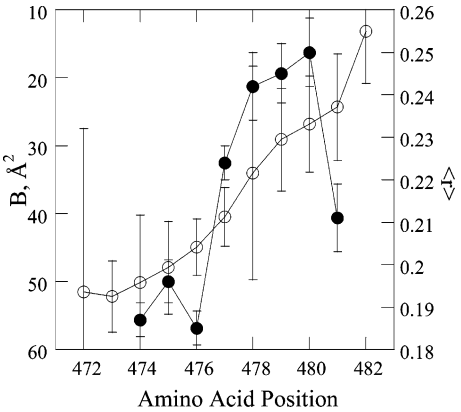

FIGURE 2: Temperature factors of Cα atoms of amino acids at the IIA^{Glc}-binding site of EcGK and steady-state anisotropies of EcGK scanning cysteine variants. The arithmetic means of the Cα temperature factors for amino acids at the IIA^{Glc}-binding site of the O, X, Y, and Z subunits of the tetramer are shown as open circles. They were taken from PDB file 1GLF, which contains the coordinates for the 2.62 Å resolution crystal structure of EcGK with glycerol and ADP bound at the active site and HPO_4^{2-} bound at the FBP site (*24*). Steady-state anisotropies obtained for OG conjugated to the scanning cysteine variants at the indicated position with 2 mM glycerol and 2.5 mM ATP are shown as filled circles. Error bars show standard deviations. Conditions: diffraction, pH 8.5−8.8; anisotropy, pH 7.0, 25 °C.

that modulates the coupling between IIA^{Glc} binding and inhibition of catalytic activity. The sequence of this locus is ...GTR... in EcGK and ...DVN... in HiGK. Figure 1 shows the locations of the coupling locus in EcGK and of the corresponding amino acids from HiGK. It is located about 15 Å from the IIA^{Glc}-binding site and about 25 Å from the active site.

The crystal structures of EcGK do not reveal the role of the coupling locus in IIA^{Glc} allosteric control. There are no van der Waals contacts or no polar interactions between the coupling locus and the IIA^{Glc}-binding site. No change of conformation of the coupling locus upon IIA^{Glc} binding is observed. Calculations by Freire and co-workers that are based on the structure of the complex show that binding of IIA^{Glc} to EcGK increases the stabilities of the amino acids at the IIA^{Glc}-binding site and, importantly, of the amino acids at the coupling locus (*27*). The crystallographic isotropic temperature factors for the region of the IIA^{Glc}-binding site that undergoes the conformational change are consistent with the mobility that may be required for the conformational change. The temperature factors of the Cα atoms of IIA^{Glc}-binding site amino acid residues for a structure of EcGK in the absence of IIA^{Glc} (*24*) are shown in Figure 2. The average temperature factor for the Cα atoms for all the residues in the protein is 24 Å^2. The temperature factors for the Cα atoms of residues 474−478, which is the region that changes conformation upon IIA^{Glc} binding, are substantially larger than the average value, suggesting this region is mobile. The apparent mobility of the IIA^{Glc}-binding site that is suggested by the temperature factors and the predicted increase of stability of the coupling locus upon IIA^{Glc} binding suggest that motions of these two regions may be related. Modulation of the motions of the IIA^{Glc}-binding site by the amino acids at the coupling locus could provide an explanation for their requirement for transplantation of allosteric inhibition into HiGK.

Molecular motions may be probed by using fluorescence anisotropy methods. Although tryptophan residues are located near the IIA^{Glc}-binding site at positions 486 and 496, intrinsic protein fluorescence of EcGK is not suitable for evaluating motions at the IIA^{Glc}-binding site. There are 13 tryptophan residues per subunit of EcGK so that isolating the contributions of 1−2 residues to the total anisotropy is problematic. The IIA^{Glc}-binding site can be targeted specifically by attaching a suitable extrinsic fluorophore to a cysteine residue that is substituted for an amino acid at the binding site. The extrinsic fluorophore OG can be conjugated specifically to the non-native cysteine residue of the E478C EcGK variant (*28*). This cysteine residue replaces the native glutamate at position 478 in the IIA^{Glc}-binding site of GK. Changes of steady-state fluorescence anisotropy of the OG resulting from homo-FRET between fluorophore molecules that are attached to different subunits were used to define the effects of FBP on the dimer−tetramer assembly reaction. Here, cysteine substitutions of amino acid 478 are constructed for HiGK and each of the chimeric GKs that were generated in the transplantation studies and for the other IIA^{Glc}-binding site amino acids 474−481 in EcGK. Solution ns dynamics of the IIA^{Glc}-binding site are examined by steady-state and time-resolved fluorescence properties of OG that is conjugated to these non-native cysteine residues. The ns dynamics of the IIA^{Glc}-binding site of EcGK in solution are consistent with the mobility that is suggested by the crystallographic temperature factors and are modified by the amino acids of the coupling locus.

MATERIALS AND METHODS

Materials. Reagents were purchased from Sigma Chemical Co. (St. Louis, MO) unless otherwise indicated. Fluorescence probes were purchased from Molecular Probes (Eugene, OR). IIA^{Glc} was generously provided by Drs. Saul Roseman and Norman D. Meadow of the Department of Biology of The Johns Hopkins University (Baltimore, MD).

Construction of Site-Directed Variants. Cysteine substitutions were constructed by using the Quick Change protocol (Stratagene, La Jolla, CA). The entire GK reading frames were confirmed for all variants by DNA sequencing. The variants containing cysteine substitutions were purified by using the same protocols that are used for the parental enzymes (*25*, *28*).

Enzyme Kinetics. GK enzyme activity was measured by using the continuous ADP-coupled spectrophotometric assay at pH 7.0 and 25 °C on a Beckman DU-640 UV/vis spectrophotometer with attached thermoelectric temperature control and a kinetics software package. The assay conditions were as described previously (*28*). Reactions were initiated by addition of enzyme to the assay cocktail. One unit of GK is defined as the amount of the enzyme that produces 1 μmol of ADP/min in this assay. The data from initial velocity studies were fit to the following equation for a sequential bisubstrate enzyme kinetics mechanism by using EnzFitter (Biosoft, Cambridge, U.K.):

$$v = \frac{V_{max}[ATP][gol]}{[ATP][gol] + K_{ATP}[gol] + K_{gol}[ATP] + K_{i,ATP}K_{gol}} \quad (1)$$

IIA^{Glc} Inhibition. IIA^{Glc} inhibition assays were performed with the presence of 2 mM glycerol, 2.5 mM ATP, and 100

μM $ZnCl_2$. The assays were initiated by the addition of enzyme. The data were fit to the following equation by using KaleidaGraph software (Synergy Software, Reading, PA):

$$\text{SA}\ (\%) = 100 - \frac{I_{\max}[\text{IIA}^{\text{Glc}}]}{K_{0.5} + [\text{IIA}^{\text{Glc}}]} \quad (2)$$

where SA is the percent remaining activity at a particular inhibitor concentration compared to the activity without inhibitor. I_{max} is the maximal percent inhibition, and $K_{0.5}$ is the apparent dissociation constant.

Labeling Glycerol Kinase with the Extrinsic Fluorophore Oregon Green. GK was equilibrated with 0.1 M TEA buffer, pH 7.0, 2 mM ATP, and 2 mM glycerol. The labeling reaction was initiated by addition of a 2-fold molar excess of IAOG in dimethylformamide, and the reaction was incubated in the dark for 1/2 h at ambient temperature before being quenched with 1 mM β-mercaptoethanol. These reaction conditions are similar to those used previously (*28*), but the pH, molar excess of label, and reaction incubation time are reduced to limit the stoichiometry of labeling. After gel permeation chromatography and dialysis overnight versus 1 L of 0.1 M TEA, pH 7.0, the glycerol kinase protein concentration was determined from absorbance at 280 nm by using the extinction coefficient 1.73 $(\text{mg/mL})^{-1}$ cm^{-1}. The stoichiometry of fluorophore incorporation was determined from the absorbance measurements at 280 and 491 nm, using the equation and the extinction coefficients supplied by Molecular Probes, Inc.

For E478C EcGK, specific labeling of the engineered cysteine residue by IAOG was shown by using HPLC to purify the OG-labeled tryptic peptide and MALDI-MS to identify it (*28*). The same methods were used here to show that the extrinsic fluorophore IAF is specifically conjugated to the engineered cysteine residue at position 478 in HiGK and its variants. These determinations were performed by the Protein Chemistry Laboratory of Texas A&M University.

Fluorescence Measurements. Emission spectra and steady-state anisotropy measurements were obtained by using an SLM-4800 spectrofluorometer equipped with Glan-Thompson calcite prism type polarizers. All measurements were done at 25 °C and using a protein concentration of 0.05 mg/mL (0.89 μM (subunits)). For the acquisition of emission spectra, the excitation wavelength was 485 nm, and the emission wavelength was scanned from 500 to 560 nm with the slit width set at 4 nm for the excitation and emission monochromators. For steady-state anisotropy determinations, the excitation wavelength was 485 nm with the slit width set at 4 nm, and an OG515 cut-on filter was used to collect the emission. The Raman scattering background was subtracted by using a blank of unlabeled GK of the same concentration. The steady-state anisotropy, $\langle r \rangle$, was calculated by using the following equation:

$$\langle r \rangle = \frac{I_{\text{VV}} - GI_{\text{VH}}}{I_{\text{VV}} + 2GI_{\text{VH}}} \quad (3)$$

where the subscript pairs H and V give the orientations (horizontal and vertical) of the excitation and emission polarizers, respectively, and $G = I_{\text{HV}}/I_{\text{HH}}$ is an instrumental correction factor (*29*).

Time-resolved fluorescence experiments were performed in the frequency domain by using a K2 multifrequency cross-correlation phase and modulation fluorometer from ISS (ISS Inc., Champaign, IL). The exciting light was from a Spectra-Physics argon ion laser tuned to 488 nm. For the lifetime measurements, the modulated beam was passed through a polarizer parallel to the vertical laboratory axis and the emission was viewed through a polarizer oriented at the magic angle (55°) to eliminate the polarization effects. Emission was collected through a Schott OG530 cut-on filter to separate the fluorescence signal from the scattered light. Experiments were performed between 2 and 250 MHz selecting 10−14 frequencies. Data were collected at each frequency until the standard deviation for each measurement of phase and modulation was below 0.2° and 0.004, respectively. To estimate fluorescence intensity decay parameters, models for the decay were fit to the frequency domain data by using Globals Analysis (DOS version 1.20; Globals Unlimited Inc., Urbana, IL). These models were evaluated: single-exponential decay, two discrete exponential decays, Gaussian distribution of decays plus single discrete exponential decay, and Lorentzian distribution of decays plus single discrete exponential decay. This analysis method returns values for the fractional contribution f_i and the lifetime τ_i for each decay phase, and the sum of f_1 and f_2 equals 1 for models with two phases. The model that best describes the data was judged by comparing the values of the fitting statistic χ^2 from the fits. For the Gaussian distribution of decays plus single-exponential decay, the average lifetime, $\bar{\tau}$, was calculated by using the equation $\bar{\tau} = f_1\tau_1 + f_2\tau_2$, where τ_1 was taken to be the center of the distribution of lifetimes (*29*).

Frequency domain anisotropy decay was measured by exciting the sample with amplitude-modulated light that passes through an excitation polarizer in the vertical orientation. The parallel components of the emission were measured by placing the emission polarizer in the vertical position, and the perpendicular components were measured by rotating the emission polarizer to the horizontal position. The anisotropy decay data were fit to a model that describes the observed decay as the sum of two exponential decays:

$$r(t) = r_0(f_1 e^{-t/\phi_1} + f_2 e^{-t/\phi_2}) \quad (4)$$

where r_0 is the anisotropy in the absence of rotational diffusion, ϕ_1 and ϕ_2 are the local and global rotational correlation times, respectively, and f_1 and f_2 are the fractional contributions of the local and global rotation to the overall anisotropy decay such that the sum of f_1 and f_2 equals 1. Fitting of the data to this model was performed by using Globals Analysis (DOS version 1.20; Globals Unlimited Inc.).

RESULTS AND DISCUSSION

Functional Properties of Glycerol Kinases with a Non-Native Cysteine Residue at the IIA^{Glc}-Binding Site. Site-specific mutagenesis was used to substitute cysteine at position 478 of HiGK and each of the chimeric GK enzymes from the IIA^{Glc} allosteric control transplantation studies and for each of the amino acids at positions 474−481 in EcGK, i.e., scanning cysteine mutagenesis. Steady-state enzyme kinetics properties and IIA^{Glc} inhibition were determined for

Table 1: Steady-State Kinetics and IIA^{Glc} Inhibition Parameters of GK Variants[a]

	kinetic parameters			IIA^{Glc} inhibition	
enzyme	V_{max} (U/mg)	K_{ATP} (μM)	K_{gol} (μM)	I_{max} (%)	$K_{0.5}$ (μM)
EcGK	14 ± 1	5 ± 2	5 ± 2	94 ± 1	0.5 ± 0.1
E478C EcGK	5 ± 1	7 ± 1	3 ± 1	86 ± 2	1.9 ± 0.2
$HiGK^{II}L$	44 ± 8	132 ± 40	43 ± 20	69 ± 1	2.0 ± 0.1
E478C $HiGK^{II}L$	18 ± 2	15 ± 8	24 ± 9	70 ± 2	2.6 ± 0.2
EcGKr	12 ± 1	4 ± 1	3 ± 1	nd	>200
E478C EcGKr	7 ± 1	3 ± 1	2 ± 1	nd	>200
HiGK	39 ± 8	89 ± 31	59 ± 27	nd	>200
K478C HiGK	21 ± 2	30 ± 12	45 ± 6	nd	>200
$HiGK^{II}$	15 ± 1	28 ± 6	15 ± 5	nd	>200
E478C $HiGK^{II}$	9 ± 1	7 ± 5	9 ± 1	nd	>200
HiGKL	47 ± 5	143 ± 28	73 ± 23	nd	>200
K478C HiGKL	18 ± 4	44 ± 25	31 ± 20	nd	>200
I474C EcGK	9 ± 1	5 ± 1	2 ± 1	70 ± 2	2.4 ± 0.2
E475C EcGK	21 ± 1	14 ± 2	9 ± 1	87 ± 2	0.6 ± 0.1
T476C EcGK	16 ± 1	17 ± 1	6 ± 1	84 ± 3	1.4 ± 0.2
T477C EcGK	24 ± 1	15 ± 3	8 ± 2	81 ± 2	1.1 ± 0.1
E478C EcGK	5 ± 1	7 ± 1	3 ± 1	86 ± 3	1.9 ± 0.2
R479C EcGK	9 ± 1	6 ± 2	2 ± 1	75 ± 3	2.3 ± 0.3
N480C EcGK	16 ± 1	31 ± 7	11 ± 5	88 ± 3	2.2 ± 0.3
Y481C EcGK	12 ± 1	17 ± 5	7 ± 3	85 ± 1	1.8 ± 0.1

[a] Kinetic and IIA^{Glc} inhibition parameters were determined as described in the Materials and Methods. Values for the chimeric GKs without the non-native cysteine at position 478 are from ref *25*. Conditions: 0.05 M TEA, pH 7.0, 25 °C. nd = not detected.

each of the purified variant enzymes as described in the Materials and Methods. Results of these studies are shown in Table 1. Two aspects of these results for the chimeric enzyme variants can be considered: effects of the cysteine substitution and effects of the coupling locus. The cysteine substitution at position 478 reduces V_{max} about 2−3-fold. It has little effect on the substrate Michaelis constants for the EcGK variants and reduces them 2−8-fold for the HiGK variants. It has small effects on the maximal inhibition (I_{max}) and apparent dissociation constant for IIA^{Glc} ($K_{0.5}$) relative to that of the respective parent enzyme for EcGK but not for $HiGK^{II}L$. The observation that the 478C substitutions have small effects on the catalytic properties indicates that the IIA^{Glc}-binding site and the catalytic site are coupled for even those enzymes that are not inhibited by IIA^{Glc}. The cysteine substitutions at 478 have only small effects on the catalytic properties and the IIA^{Glc} inhibition, indicating that these variant enzymes are suitable for evaluation of the dynamics properties of the IIA^{Glc}-binding site. This conclusion is further supported by the X-ray crystal structure of the IIA^{Glc}−E478C EcGK complex (*30*). The only change seen for this structure relative to that of the native EcGK complex is the difference between glutamate and cysteine at the site of the substitution.

The amino acid substitutions at the coupling locus have very small effects on the catalytic properties of the EcGK or HiGK enzymes, and this is seen for the enzymes with and without the non-native cysteine residue at 478. Changing the coupling locus amino acids of the $HiGK^{II}$ enzymes has larger effects on the catalytic properties. The V_{max} and Michaelis constants for both substrates are increased 2−3-fold by the coupling locus amino acids from EcGK for enzymes with and without the non-native cysteine residue at 478. The substitution of the sequentially contiguous IIA^{Glc}-binding site amino acids from EcGK to generate the $HiGK^{II}$ chimeric enzyme reduces the V_{max} and Michaelis constants to near those of the EcGK enzyme, and the additional substitution of the coupling locus amino acid residues to generate the $HiGK^{II}L$ enzyme returns these parameters to near those of the parent HiGK. The effects of these changes in coupling locus amino acids indicate that the coupling locus indeed modulates coupling between the IIA^{Glc}-binding site and the active site.

The catalytic and IIA^{Glc} inhibition properties of the scanning cysteine variant enzymes are also shown in Table 1. These properties are similar to one another and to EcGK. The maximum extent of IIA^{Glc} inhibition (I_{max}) is reduced for the I474C and R479C variants. Similar results were obtained for the I474A and R479A variants (*31*). The small effects of these scanning cysteine substitutions on the catalytic and allosteric properties indicate that these variants should provide meaningful insights into the dynamics properties of the IIA^{Glc}-binding site.

Extrinsic Fluorophore Labeling of the Non-Native Cysteine Residues. The non-native cysteine residue at the IIA^{Glc}-binding site of each of these GK variants allows reaction with IAOG for covalent attachment of the extrinsic fluorophore OG. No labeling with IAOG is observed for the wild-type enzyme EcGK or HiGK under these conditions. This result suggests that the labeling that is observed for the variant enzymes reflects OG that is conjugated to the non-native cysteine residue. The non-native cysteine residue of the E478C EcGK variant is labeled specifically by IAOG (*28*). The site of modification of the K478C HiGK variant by IAF was determined for these studies as described in the Materials and Methods. The results of those determinations confirm the specific modification of the non-native cysteine residue by the fluorophore. Because each of the parent 478C enzymes is modified specifically at the non-native cysteine residue under the reaction conditions that are used in these studies, we assume this is the case for the remaining enzymes. This assumption is supported by the results of steady-state anisotropy experiments that are described below.

For most of these studies, the conjugated fluorophore stoichiometry was controlled in the range of 0.05−0.1 mol of OG/mol of GK subunit by using the reaction conditions that are described in the Materials and Methods. This low stoichiometry further avoids modification of the native cysteine residues and eliminates effects on the anisotropy from homo-FRET between fluorophores that are attached to different subunits of the same GK oligomer. In addition, the fluorophore is most likely a reporter of events in a single subunit of the protein oligomer. Both EcGK and HiGK form dimers and tetramers in solution (*26*), but no homotropic interactions have been observed for IIA^{Glc} inhibition.

Emission spectra of the OG-labeled GK variants were recorded from 500 to 560 nm with excitation at 485 nm. The concentrations of the labeled variants were adjusted to give the same absorbance at 485 nm for comparison of the spectra. The shape of the spectrum and the wavelength of the maximum emission (518 ± 2 nm) are similar for all of the variant enzymes (not shown). The intensity at the maximal wavelength varies by about 3-fold. The highest intensity is observed for the E475C EcGK and E478C $HiGK^{II}L$ variants, and the lowest intensity is observed for the E478C EcGK and E478C $HiGK^{II}$ variants. The intensity for each of the labeled variant enzymes is substantially less

Table 2: Steady-State and Time-Resolved Fluorescence Properties of OG-Labeled Chimeric GK Variants[a]

enzyme	⟨r⟩	lifetime f_1	τ_1 center (ns)	τ_1 width (ns)	τ_2 (ns)	lifetime $\bar{\tau}$ (ns)	lifetime χ^2	TRFA f_1	TRFA ϕ_1 (ns)	TRFA χ^2
E478C EcGKr	0.215 ± 0.004	0.91 ± 0.01	3.67 ± 0.08	0.91 ± 0.13	0.54 ± 0.04	3.39 ± 0.09	0.54	0.53 ± 0.01	0.42 ± 0.03	0.90
E478C EcGK	0.241 ± 0.005	0.93 ± 0.01	3.74 ± 0.07	0.85 ± 0.12	0.78 ± 0.05	3.52 ± 0.09	0.39	0.41 ± 0.03	0.52 ± 0.12	1.23
E478C HiGK^{II}	0.170 ± 0.004	0.91 ± 0.01	4.02 ± 0.04	0.87 ± 0.11	0.59 ± 0.04	3.71 ± 0.06	0.58	0.51 ± 0.01	0.26 ± 0.01	0.22
E478CHi GK^{II}L	0.226 ± 0.003	0.95 ± 0.01	4.12 ± 0.04	0.68 ± 0.11	0.85 ± 0.05	3.96 ± 0.06	1.06	0.33 ± 0.01	0.29 ± 0.02	0.78
K478C HiGK	0.268 ± 0.005	0.97 ± 0.01	4.36 ± 0.04	0.72 ± 0.17	0.84 ± 0.06	4.25 ± 0.07	0.74	0.21 ± 0.01	0.08 ± 0.02	0.56
K478C HiGKL	0.263 ± 0.005	0.96 ± 0.01	4.35 ± 0.04	0.59 ± 0.18	0.99 ± 0.07	4.22 ± 0.08	0.96	0.25 ± 0.01	0.08 ± 0.02	0.43

[a] Steady-state and time-resolved fluorescence anisotropy parameters were determined as described in the Materials and Methods. Conditions: 0.1 M TEA, 2 mM glycerol, pH 7.0, 25 °C.

than the intensity from the same concentration of OG in solution. For all of the OG-labeled enzymes, the maximum wavelength of the absorbance spectrum is red-shifted to about 500 nm. A similar red shift was seen for other OG-labeled proteins (*32*) and for fluorescein bound to anti-fluorescein Fab fragments (*33*). The reduced intensity and red-shifted absorbance spectrum relative to those of OG in solution indicate interactions between the conjugated fluorophore and the protein which alter the ground state of the fluorophore. The differences of emission intensity observed for the scanning cysteine enzymes indicate that these interactions depend on the site of conjugation, while the differences obtained for the chimeric enzymes indicate that the interactions depend on the flanking primary structure of the conjugation site and the coupling locus.

Steady-State Fluorescence Anisotropies of the OG-Labeled Enzymes Are Consistent with Modulation of Local ns Dynamics by the Coupling Locus. Steady-state anisotropies, ⟨*r*⟩ given by eq 3, were measured for each of the OG-labeled variant enzymes. At least three independent labeling experiments were performed for each enzyme, and the steady-state anisotropies that are reported are the arithmetic mean ± standard deviation from those determinations. The steady-state anisotropies of OG that is conjugated to the non-native cysteine residue at position 478 of the chimeric GKs are shown in Table 2. The values range from 0.268 to 0.170, depending on the sequences flanking the site of fluorophore attachment and on the sequence at the coupling locus. Roles of different protein structural elements can be evaluated by comparing steady-state anisotropies for the members of each pair of enzymes that differ from one another only at the coupling locus: the EcGK pair (E478C EcGKr and E478C EcGK), the HiGK^{II} pair (E478C HiGK^{II} and E478C HiGK^{II}L), and the HiGK pair (K478C HiGK and K478C HiGKL), where the first member of each pair has the coupling locus sequence from HiGK and the second member has the coupling locus sequence from EcGK. The anisotropies for the EcGK and HiGK^{II} enzyme pairs, which have the IIA^{Glc}-binding site amino acids from EcGK, are smaller than those for the HiGK pair. For the EcGK and HiGK^{II} enzyme pairs, the anisotropy is higher for the enzyme with the coupling locus sequence from EcGK. The anisotropy for the HiGK enzyme pair shows little dependence on the coupling locus sequence. To the extent that the steady-state anisotropies reflect local fluorophore motions, these results suggest that the IIA^{Glc}-binding site is mobile and the mobility is altered by the coupling locus amino acids. The mobility at position 478 in the IIA^{Glc}-binding site appears to be decreased by the coupling locus amino acids from EcGK, as seen from the increased steady-state anisotropies.

Steady-state anisotropies for the scanning cysteine variants are shown in Figure 2 and range from about 0.25 to 0.19 depending on the position to which the fluorophore is conjugated. Smaller values of anisotropy are obtained for OG that is conjugated to the I474C, E475C, and T476C EcGK variants, positions which show the IIA^{Glc}-dependent conformational change, and higher anisotropies are obtained for the remaining variants. The value of the steady-state anisotropy that is obtained for the OG conjugated to positions 474−480 is highly correlated with the isotropic temperature factor for the backbone Cα atom. An unweighted linear least-squares fit for a plot of anisotropy versus temperature factor for these amino acid positions has a correlation coefficient (R^2) of 0.903. This high correlation is consistent with local motions as the basis for the differences in steady-state anisotropy and strongly suggests that the steady-state fluorescence anisotropy of the conjugated extrinsic fluorophore monitors the protein backbone motions of the IIA^{Glc}-binding site. The good correlation is also consistent with the expected specific labeling by OG at each of the scanning cysteine variant sites.

For all of the labeled variant enzymes, the steady-state anisotropy is reduced by 0.005−0.015 upon binding of the active site ligands ATP and glycerol (not shown). The dependence of the anisotropy on ligand binding to the active site more than 30 Å from the IIA^{Glc}-binding site shows that these enzyme regions are coupled for even those enzymes that are not inhibited by IIA^{Glc}. The reductions in steady-state anisotropies by ligand binding are consistent with increased local motions at the IIA^{Glc}-binding site. The allosteric coupling between ATP and IIA^{Glc} was determined for the E478C EcGK and E478C HiGK^{II}L enzymes by using steady-state enzyme kinetics. Those studies show cooperative interactions between these two ligands such that each increases the apparent affinity for the other by about 4-fold (D. W. Pettigrew, manuscript in preparation). This heterotropic coupling is consistent with the ATP effects on local motions at the IIA^{Glc}-binding site.

The differences in steady-state anisotropies that are obtained for each of these GK enzymes could arise from differences in homo-FRET, global and/or local rotations, and/or fluorescence lifetimes. The low labeling stoichiometry (0.05−0.1 mol of OG/mol of GK subunit) prevents multiply labeled GK oligomers and eliminates effects of homo-FRET on the steady-state anisotropies (*28*). The subunit molecular mass of both HiGK and EcGK is about 56 kDa, and both enzymes form dimers and tetramers in solution (*26*). Mean rotational correlation times for the EcGK dimer and tetramer were calculated by using the computer program HYDRO-PRO (*34*) with the structure coordinates from PDB file 1BO5

(*35*). These calculations yield mean rotational correlation times for the EcGK dimer and tetramer of 120 and 150 ns, respectively, and the same values should obtain for HiGK due to the high sequence identity/similarity. These global rotational correlation times are much longer than the reported lifetimes for OG intensity decay: 3.8 ± 0.1 ns for the IAOG−mercaptoethanol adduct in aqueous buffer (*32*) and 4.04 ± 0.06 ns for OG in aqueous solution (*36*). Thus, these large proteins are effectively immobile in terms of global rotations during the lifetime of the excited state. Moreover, the global rotational correlation times are the same for all of these enzymes, eliminating differences in global rotation as the basis for differences in steady-state anisotropies seen for different variants. The observed steady-state anisotropies are all less than the r_0 value of 0.383 for OG (*32*), indicating that the fluorophore is not completely immobilized, but they are all greater than 0, indicating that the motions of the fluorophore are restricted.

Differences in Fluorescence Lifetimes Do Not Account for Differences in Steady-State Anisotropies. The ranges of emission intensities and steady-state fluorescence anisotropies that are observed for the different enzymes may reflect differences in the fluorescence lifetimes of the conjugated extrinsic fluorophores. Lifetimes were determined by using frequency domain time-resolved fluorescence intensity decay methods. For these methods, differences in fluorescence lifetimes are observed as shifts of the frequency dependencies of the phase and modulation, where a shift to higher frequencies indicates a decreased lifetime and/or fraction of the decay. The points in Figure 3 show the frequency domain fluorescence decay data that were obtained for the chimeric GK enzymes and the scanning cysteine variant enzymes, respectively. The data show only small differences in the phase shift and modulation, indicating that the lifetimes and/or fractional contributions to the decay are very similar. This conclusion is supported by the time-resolved parameters that are obtained from fitting of the data.

Fluorescence lifetimes were determined from fitting the decay data that are shown in Figure 3 to different decay models. The data are not well described by either a single or double discrete exponential decay model, with the exception of data for the E475C EcGK variant. In all cases, the best fit to the decay is obtained by using a model with two components: a distribution of exponential decays and a discrete exponential decay with a shorter lifetime. For the distribution of decays, a better fit is obtained for a Gaussian distribution than for a Lorentzian distribution. For the chimeric GK variants, each data set was fit independently to this model. The data for the scanning cysteine variant enzymes were fit simultaneously to this model, with the values for the emission relaxation time for the discrete component, τ_2, linked for all the data sets. The lines in Figure 3 show the fits of the data to this decay model, and the parameters that are obtained from the fits are shown in Tables 2 and 3. The values for the fitting statistic χ^2 as well as the good agreement between the fitted lines and the data points in Figure 3 show that this model provides a good description of the fluorescence decay. More than 90% of the fluorescence decay is accounted for by the processes associated with the distribution of lifetimes. There is little difference between the distributions of the lifetimes. The centers of the distribution of lifetimes range from 3.7 ± 0.08 to 4.36 ± 0.04 ns,

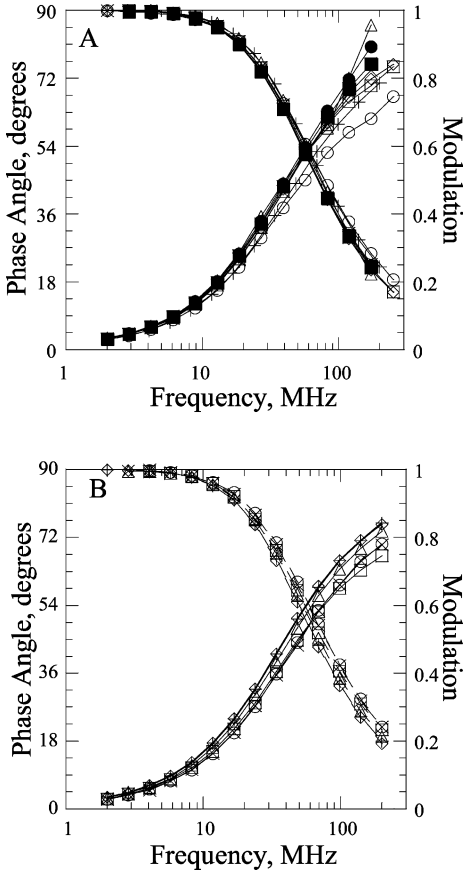

FIGURE 3: Frequency domain determination of the fluorescence lifetimes of the OG-labeled GKs. The plots show the excitation light modulation frequency dependencies of the phase shift and modulation for the fluorescence emission. Points show the data, and lines show the fit to a model using a discrete lifetime plus a Gaussian distribution of lifetimes to describe the observed phase shift and modulation. Parameters obtained from the fits are shown in Tables 2 and 3. Conditions: 0.1 M TEA, 2 mM glycerol, pH 7.0, 25 °C. (A) Chimeric enzymes. Key: open circles, E478C EcGK; times signs, E478C EcGKL; open squares, E478C HiGK^{II}; open triangles, E478C HiGK^{II}L; open tilted squares, K478C HiGK; plus signs, K478C HiGKL; solid lines, phase shift; dashed lines, modulation. (B) Scanning cysteine variant enzymes. Key: open circles, I474C; open squares, E475C; open tilted squares, T476C; times signs, T477C; plus signs, E478C; triangles, R479C; filled circles, N480C; filled squares, Y481C.

Table 3: Fluorescence Lifetimes of the OG-Labeled Scanning Cysteine EcGK Variants[a]

enzyme	f_1	τ_1 center (ns)	τ_1 width (ns)	τ_2 (ns)	χ^2
I474C EcGK	0.912 ± 0.011	4.03 ± 0.03	0.91 ± 0.13	0.60	1.19
E475C EcGK	0.942 ± 0.004	4.04 ± 0.02	0.02 ± 0.16	0.60	1.11
T476C EcGK	0.960 ± 0.008	4.09 ± 0.02	0.62 ± 0.14	0.60	0.44
T477C EcGK	0.928 ± 0.012	4.02 ± 0.02	0.55 ± 0.15	0.60	0.24
E478C EcGK	0.945 ± 0.010	3.87 ± 0.04	0.88 ± 0.13	0.60	0.46
R479C EcGK	0.969 ± 0.011	3.92 ± 0.04	1.04 ± 0.13	0.60	0.69
N480C EcGK	0.962 ± 0.004	3.88 ± 0.02	0.87 ± 0.12	0.60	0.73
Y481C EcGK	0.970 ± 0.003	4.03 ± 0.02	0.91 ± 0.06	0.60	0.74

[a] The GK variants were labeled with OG to a stoichiometry of ~0.1 mol of OG/mol of GK subunit. Conditions: 0.1 M TEA, pH 7.0, 2 mM glycerol, 25 °C.

which is in good agreement with the reported lifetimes for OG decay: 3.8 ± 0.1 ns for the IAOG−mercaptoethanol adduct in aqueous buffer (*32*) and 4.04 ± 0.06 ns for OG in aqueous solution (*36*). The widths of the decay distributions

are similar for all of the GKs, with the exception of the E475C EcGK variant, for which the width is small. For this variant, the decay data are well-described also by a model with two discrete exponentials. The fraction of the decay that is described by processes associated with the distribution of lifetimes ranges from 0.91 to 0.97.

The remainder of the fluorescence decay is described by a discrete sub-ns lifetime. This shorter lifetime shows a range of about 2-fold (0.54−0.99 ns) for the chimeric GK variants. These values agree well with the value of 0.6 ns that was obtained from the linked fits for the scanning cysteine variant GKs. The basis for this short discrete lifetime is unknown. Multiexponential intensity decays are not observed for OG in neutral solution (*32*, *36*). At lower pH and with acetate buffer, decay processes with sub-ns lifetimes that are attributed to excited-state proton transfer are reported for OG in aqueous solution (*36*). Sub-ns lifetime components are observed for fluorescein that is bound to anti-fluorescein Fab fragments (*33*). The similarities of the values for this short lifetime that are obtained for all of the GK variant enzymes show that all of the environments of the conjugated OG are similar and/or this lifetime shows little dependence on the environment. The differences in emission intensities suggest that not all of the environments are the same.

The differences in fluorescence emission intensities are somewhat correlated with the values of the centers of the distributions of lifetimes. Higher emission intensities are associated with longer lifetimes. However, I474C EcGK and HiGK^{II} show lower emission intensity despite having longer lifetimes, indicating that factors other than lifetimes are influencing the emission intensities. The differences in the lifetimes for variants that show very different emission intensities are small in any case. For the scanning cysteine variants, the lifetimes that are obtained for the variants with the highest and lowest emission intensities are 4.04 ± 0.04 ns for E475C EcGK and 3.87 ± 0.04 ns for E478C EcGK, respectively, while the emission intensities differ by about 3-fold.

The differences in fluorescence lifetimes that are observed for these variant GKs do not account adequately for the differences in steady-state anisotropies. For the scanning cysteine variants, the centers of the distributions of the fluorescence lifetimes range from 3.87 ± 0.04 to 4.09 ± 0.02 ns. As expected, shorter lifetimes are associated with larger steady-state anisotropies. The decreases of lifetime are about 0.1 ns. If the local rotational correlation time for OG that is attached to these cysteine residues is in the sub-ns range that is seen below for the chimeric GKs, then the Perrin equation predicts that a lifetime decrease of 0.1 ns will increase the steady-state anisotropy by about 0.008 (*29*). The observed increase of steady-state anisotropy is much larger, about 0.06.

The centers of the distributions of lifetimes for the chimeric enzymes range from 3.67 ± 0.08 to 4.36 ± 0.04 ns. For each pair of enzymes that differ only at the coupling locus, the values of the centers of the distributions are the same, but there are small differences for the value of f_1, the contribution of the distribution of lifetimes to the intensity decay. The contribution of the shorter, discrete lifetime decay process differs for each member of each enzyme pair. The average lifetime, $\bar{\tau}$, was calculated as described in the Materials and Methods and is shown in Table 2. It reflects the contribution of both of the decay components to the overall fluorescence decay. Its value ranges from 3.4 to 4.3 ns and displays the same relative order as the centers of the distributions of lifetimes. It is different for each member of the pairs of enzymes that differ only at the coupling locus sequence. For example, the average lifetime is decreased for E478C HiGK^{II} relative to E478C HiGK^{II}L, reflecting the small decrease in the value of the center of the distribution of lifetimes and the decrease in the lifetime of the discrete component. The shorter lifetime is expected to result in increased steady-state anisotropy, but it is decreased substantially for E478C HiGK^{II} relative to E478C HiGK^{II}L. Similar results are seen for the other chimeric enzymes. In all cases, the effect of the coupling locus on the steady-state anisotropies is opposite its expected effect on the fluorescence lifetimes.

The effects of the coupling locus on the steady-state anisotropies for OG that is conjugated to non-native cysteine residues at the IIA^{Glc}-binding site of EcGK thus are not due to differences in homo-FRET, global rotation, or fluorescence lifetimes. The steady-state anisotropies for the extrinsic fluorophore report on the local protein motions at the site, and those motions are modulated by the amino acids at the coupling locus which is located more than 15 Å away.

Characterization of the Effects of the Coupling Locus on the Motions of the IIA^{Glc}-Binding Site. The local fluorophore motions for the chimeric enzymes and the effects of the coupling locus sequence on them were characterized by using frequency domain time-resolved fluorescence anisotropy methods. In this experimental approach, the rates of the fluorophore motions that are associated with anisotropy decay can be directly related to the modulation frequency of the exciting light; fast and slow rates of motion are observed at high and low modulation frequencies, respectively. The extent of the contribution of the local motions to the anisotropy decay is related to their amplitudes.

Data that were obtained from the frequency domain time-resolved fluorescence anisotropy studies of the chimeric GK variants are shown by the points in Figure 4. This figure shows the dependencies on the modulation frequency of the exciting light for the differential phase shift and for the ratio of the modulated amplitudes of the vertical and horizontal emission components. These data indicate that a portion of the anisotropy decay is associated with fluorophore motions that are characterized by very short rotational correlation times. The ratios of the modulated amplitudes depend little on the excitation modulation frequencies below about 70 MHz, indicating that rotational correlation times of less than 1 ns are associated with the anisotropy decay. The differences in the ratio of the modulated amplitudes of the emission components at the lower frequencies mirror the differences in steady-state anisotropy. The measured values of the modulation ratio at the lowest frequency are highly correlated with the independently determined values of the steady-state anisotropy ($R^2 = 0.894$). This good correlation provides confidence in the validity of the time-resolved anisotropy decay data. The validity of the data was evaluated by replicate measurements with the same preparation on the same day, which showed excellent agreement. There was greater variation among results obtained for independent preparations, which are considered below.

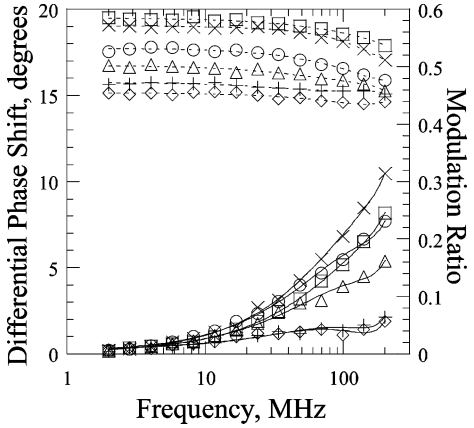

FIGURE 4: Frequency domain time-resolved fluorescence anisotropy for the OG-labeled chimeric GKs. The plot shows the excitation light modulation frequency dependencies of the differential phase shift and ratio of the modulation of the parallel and perpendicular components of the anisotropy decay. Points show the data, and lines show the fit to eq 4, a model in which two rotational components (one global and the other local) contribute to the total anisotropy decay. Parameters obtained from the fits are shown in Table 2. Conditions: 0.1 M TEA, 2 mM glycerol, pH 7.0, 25 °C. Key: open circles, E478C EcGK; times signs, E478C EcGKr; open squares, E478C HiGK^{II}; open triangles, E478C HiGK^{II}L; open tilted squares, K478C HiGK; plus signs, K478C HiGKL; solid lines, differential phase shift; dashed lines, modulation ratio.

To obtain the local rotational correlation times, the time-resolved fluorescence anisotropy data in Figure 4 were fit to eq 4 as described in the Materials and Methods. The parameters from the best fitting model for the total intensity decay, a Gaussian distribution of lifetimes plus a discrete exponential, were used for the fits, and intensity decay times were not associated with correlation times (*37*, *38*). The value for r_0 was fixed to 0.38, the value reported for OG (*32*), giving a constrained analysis that was shown to result in improved parameter estimates from anisotropy decay data (*39*). Results of initial fits yielded a global rotational correlation time, ϕ_2, of about 75 ns with a broad range of uncertainty for all of the enzymes. This value for ϕ_2 is about the value that is expected for a spherical molecule of about 120 kDa molecular mass but is less than the mean rotational correlation time of 120 ns that is calculated for the asymmetric EcGK dimer from the crystal structure (*35*) by using HYDROPRO (*34*). The EcGK and HiGK enzymes are primarily dimeric under these conditions (*26*). The effect on the fitted parameters of fixing the value for ϕ_2 over the range of values bound by the uncertainties that were obtained from the initial fittings was investigated. The values for f_1 and ϕ_1 are not significantly affected by the value of ϕ_2 over this range. This lack of sensitivity is expected because these values of ϕ_2 are much larger than the lifetimes of the conjugated fluorophores so that the global rotation has little effect on these properties of the local rotation. However, the larger values for ϕ_2 increase the values of the fitting statistic χ^2. For the final data fitting, the value of ϕ_2 was fixed to 75 ns for all of the enzymes. The lines in Figure 4 show the fit of the data to eq 4, and the parameters that are obtained from the fit are shown in Table 2. The data are well-described by this two-exponential decay model, as shown by the values of the fitting statistic χ^2 and the uncertainties in Table 2, as well as by the good agreement between the data and the lines in Figure 4. The values of the local rotational correlation time, ϕ_1, are sub-ns, as expected from inspection of the data, and show a range of about 5-fold. The values of the contribution of the local rotational correlation time to the anisotropy decay, f_1, range from 0.21 to 0.53. Thus, there are substantial differences in the local motions of the OG fluorophores that are conjugated at the same position in the chimeric GK variants, as expected from examination of the steady-state anisotropies.

For all three enzyme pairs, the local correlation times that are associated with the anisotropy decay are very short, with values of less than 1 ns. The value is different for each pair of enzymes that differ only at the coupling locus but is the same for each member of a pair. Thus, the correlation times for the rapid motions are not modulated by the amino acid residues at the coupling locus. The local rotational correlation time is very short for the HiGK enzyme pair. The estimates of these very short times doubtless are less certain than indicated from the ranges of uncertainty returned by the fitting programs because they occur at the upper end of the frequency range. However, the short times are consistent with the results expected from simple inspection of the data, which differ markedly from those of the other two enzyme pairs. The much shorter time that is seen for the HiGK enzyme pair relative to the other two pairs shows that the local rotational correlation times depend on the primary structure that is flanking the site of conjugation at residue 478. The flanking primary structure is the same for the enzymes with the IIA^{Glc}-binding site from EcGK (the EcGK and HiGK^{II} pairs), but different local rotational correlation times of 0.52 $\pm$ 0.1 and 0.28 $\pm$ 0.02 ns, respectively, are observed for these pairs. This difference indicates that protein regions beyond the flanking primary structure also affect these correlation times.

The amplitudes of the rapid anisotropy decay, f_1, are modulated by the amino acid residues at the coupling locus, and the effect depends on the flanking primary structure. For the HiGK enzyme pair, f_1 is smaller than for either of the other two enzyme pairs and is slightly larger for HiGKL, the enzyme with the coupling locus from EcGK. Neither member of the HiGK enzyme pair is inhibited by IIA^{Glc}, and the effect of the change in coupling locus on f_1 is much smaller for this pair of enzymes than for the other two pairs. For the HiGK^{II} and EcGK enzyme pairs, the larger value of f_1 is seen for the enzymes with the coupling locus sequence from HiGK (E478C HiGK^{II} and E478C EcGKr). Although all four of these enzymes contain the amino acid residues of the crystallographically identified EcGK IIA^{Glc}-binding site, only the enzymes with the coupling locus sequence from EcGK are inhibited by IIA^{Glc}, and that inhibition is associated with a reduced contribution of the local motions to the anisotropy decay, i.e., reduced f_1. For each pair of enzymes, the larger value for f_1 is associated with the smaller steady-state anisotropy. Thus, the steady-state anisotropies reflect primarily the local motions. The results that are shown for EcGK are the average from two different preparations for which measurements were performed several weeks apart. Variation between preparations increases the ranges of uncertainty for the parameters but does not alter the conclusions reached here.

The description of the anisotropy decay by two exponentials indicates that the shorter rotational correlation time must be associated with a limited depolarization, i.e., a hindered

rotation. In such cases, the motions are often modeled as rotation within a cone where the cone angle, Φ, describes the amplitude of the hindered motion (*9*, *40*). In the context of this model, reductions of f_1 are associated with reduced values for Φ. For the two pairs of enzymes with the IIA^{Glc}-binding site amino acids, the enzyme that is inhibited by IIA^{Glc} has the coupling locus sequence from EcGK and shows the smaller value for f_1. The EcGK coupling locus thus reduces the amplitude of the local motions, tuning them to enable IIA^{Glc} binding and inhibition. The observation of larger values for f_1, i.e., larger amplitudes of the local motions, for the enzymes which are not inhibited by IIA^{Glc} suggests an unfavorable entropic contribution for IIA^{Glc} binding.

The good correlation between the steady-state anisotropies and isotropic temperature factors for the Cα atoms of the scanning cysteine variant enzymes strongly suggests that the OG that is conjugated to these non-native cysteine residues reports on the motions of the backbone atoms of this region. In this case, the sub-ns rotational correlation times reflect those motions. A similar conclusion is reported for sub-ns motions of non-native tryptophan residues in a loop of TetR (*41*) and from molecular dynamics simulations of the Alexa488 fluorophore that is conjugated to a loop of bacteriorhodoposin (*42*). The molecular dynamics simulations indicate that conjugation of the fluorophore does not significantly alter the motions of the protein.

Summary and Conclusions. The non-native cysteine residue that replaces the different native amino acid residues in the IIA^{Glc}-binding site of the GKs does not much affect the catalytic or IIA^{Glc} inhibitory properties of the enzyme. This cysteine residue is specifically labeled by reaction with IAOG under reaction conditions that yield a reporter for a single subunit of the oligomeric enzyme. The emission intensity and steady-state anisotropy of the conjugated extrinsic fluorophore depend on the site of conjugation, but the fluorescence lifetime of the probe shows little dependence on the site of conjugation. A substantial red shift of the absorbance spectrum and reduced emission intensity relative to those of OG in solution is observed for OG that is conjugated to all of the variant enzymes, strongly suggesting interactions between the bound probe and the protein, yet the emission decay is dominated by the decay modes of OG that are seen for the isolated fluorophore in solution for all enzymes. The steady-state anisotropy of the probe reflects primarily the local motions of the protein backbone to which the fluorophore is conjugated, which are clearly different for different sites and dependent on the amino acids at the coupling locus. The effects of the cysteine substitutions on the catalytic parameters and effects of substrate binding on steady-state anisotropies for all of the variants, including those that are not inhibited by IIA^{Glc}, show that the allosteric and active sites are coupled for all of these enzymes. Acquisition of allosteric inhibition by IIA^{Glc} for the enzymes E478C EcGK and E478C $HiGK^{II}L$ relative to E478C EcGKr and E478C $HiGK^{II}$ is associated with increased steady-state anisotropies, which is consistent with reduced local motions. Time-resolved fluorescence anisotropy shows that the amplitude of the local motions is reduced while the rotational correlation time is not changed. Thus, the coupling locus modulates the protein dynamics at the IIA^{Glc}-binding site. These distal effects of amino acids in a communications network that couples that site to the catalytic site are consistent with views of allostery discussed in recent reviews (*1*−*3*). This experimentally observed coupling between the amino acids of the coupling locus and the dynamics/stability of the IIA^{Glc}-binding site is consistent with the effect of IIA^{Glc} binding on the stability of the amino acids at the coupling locus that is seen in the calculations of Freire and co-workers (*27*).

Recent studies of the roles of dynamics in allosteric behavior utilize NMR methods to measure the dynamics of the NtrC receiver domain (*11*), the ATP-binding cassette of an ABC transporter (*12*), and the PDZ domain derived from human protein tyrosine phosphatase 1E (*10*). Those studies provide a clear demonstration of ligand-dependent changes in protein dynamics which are consistent with allosteric signaling. However, because the proteins in those studies are not intact, the effect of changes in the dynamics on the signaling could not be directly assessed. Here, these GKs are intact proteins, and the changes in local protein dynamics can be directly related to binding of the allosteric effector.

REFERENCES

1. Swain, J. F., and Gierasch, L. M. (2006) The changing landscape of protein allostery, *Curr. Opin. Struct. Biol. 16*, 102−108.
2. Kern, D., and Zuiderweg, E. R. P. (2003) The role of dynamics in allosteric regulation, *Curr. Opin. Struct. Biol. 13*, 748−757.
3. Freire, E. (1998) Statistical thermodynamic linkage between conformational and binding equilibria, *Adv. Protein Chem. 51*, 255−279.
4. Weber, G. (1972) Ligand binding and internal equilibria in proteins, *Biochemistry 11*, 864−878.
5. Ortigosa, A. D., Kimmel, J. L., and Reinhart, G. D. (2004) Disentangling the web of allosteric communication in a homotetramer: Heterotropic inhibition of phosphofructokinase from *Bacillus stearothermophilis*, *Biochemistry 43*, 577−586.
6. Fenton, A. W., Paricharttanakul, N. M., and Reinhart, G. D. (2004) Disentangling the web of allosteric communication in a homotetramer: Heterotropic activation in phosphofructokinase from *Escherichia coli*, *Biochemistry 43*, 14104−14110.
7. Wand, A. J. (2001) Dynamic activation of protein function: A view emerging from NMR spectroscopy, *Nat. Struct. Biol. 8*, 926−931.
8. Gunasekaran, K., Ma, B., and Nussinov, R. (2004) Is allostery an intrinsic property of *all* dynamic proteins? *Proteins: Struct., Funct., Bioinf. 57*, 433−443.
9. Johnson, J. L., and Reinhart, G. D. (1994) Influence of substrates and MgADP on the time-resolved intrinsic fluorescence of phosphofructokinase from *Escherichia coli*. Correlation of tryptophan dynamics to coupling entropy, *Biochemistry 33*, 2644−2650.
10. Fuentes, E. J., Der, C. J., and Lee, A. L. (2004) Ligand-dependent dynamics and intramolecular signaling in a PDZ domain, *J. Mol. Biol. 335*, 1105−1115.
11. Volkman, B. F., Lipson, D., Wemmer, D. E., and Kern, D. (2001) Two-state allosteric behavior in a single-domain signaling protein, *Science 291*, 2429−2433.
12. Wang, G., Karpowich, N., Hunt, J. F., Rance, M., and Palmer, A. G. I. (2004) Dynamics of ATP-binding cassette contribute to allosteric control, nucleotide binding, and energy transduction in ABC transporters, *J. Mol. Biol. 342*, 525−537.
13. Postma, P. W., Lengeler, J. W., and Jacobson, G. R. (1993) Phosphoenolpyruvate:carbohydrate phosphotransferase systems of bacteria, *Microbiol. Rev. 57*, 543−594.
14. Roseman, S. (1994) in *Phosphate in Microorganisms: Cellular and Molecular Biology* (Silver, S., Ed.) pp 151−160, ASM Press, Washington, DC.
15. Hogema, B. M., Arents, J. C., Bader, R., Eijkemans, K., Yoshida, H., Takahashi, H., Alba, H., and Postma, P. W. (1998) Inducer exclusion in *Escherichia coli* by non-PTS substrates−The role of the PEP to pyruvate ratio in determining the phosphorylation state of enzyme IIA^{Glc}, *Mol. Microbiol. 30*, 487−498.

16. Hurley, J. H., Faber, H. R., Worthylake, D., Meadow, N. D., Roseman, S., Pettigrew, D. W., and Remington, S. J. (1993) Structure of the regulatory complex of *Escherichia coli* III^{Glc} with glycerol kinase, *Science 259*, 673−677.
17. http://ca.expasy.org/uniprot/P0A6F3.
18. Bennett, W. S., and Steitz, T. A. (1980) Structure of a complex between yeast hexokinase A and glucose, *J. Mol. Biol. 140*, 211−230.
19. Grueninger, D., and Schulz, G. E. (2006) Structure and reaction mechanism of L-rhamnulose kinase from *Escherichia coli*, *J. Mol. Biol. 359*, 787−797.
20. Yeh, J. I., Charrier, V., Paulo, J., Hou, L., Darbon, E., Claiborne, A., Hol, W. G. J., and Deutscher, J. (2004) Structures of *Enterococcal* glycerol kinase in the absence and presence of glycerol: Correlation of conformation to substrate binding and a mechanism of activation by phosphorylation, *Biochemistry 43*, 362−373.
21. Anderson, M. J., DeLaBarre, B., Raghunathan, A., Palsson, B. O., Brunger, A. T., and Quake, S. R. (2007) Crystal structure of a hyperactive *Escherichia coli* glycerol kinase mutant Gly230 to Asp obtained using microfluidic crystallization devices, *Biochemistry 46*, 5722−5731.
22. Bystrom, C. E., Pettigrew, D. W., Branchaud, B. P., O'Brien, P., and Remington, S. J. (1999) Crystal structures of *Escherichia coli* glycerol kinase variant S58W in complex with nonhydrolyzable ATP analogues reveal a putative active conformation of the enzyme as a result of domain motion, *Biochemistry 38*, 3508−3518.
23. Hurley, J. H. (1996) The sugar kinase/heat shock protein 70/actin superfamily: Implications of conserved structure for mechanism, *Annu. Rev. Biophys. Biomol. Struct. 25*, 137−162.
24. Feese, M. D., Faber, H. R., Bystrom, C. E., Pettigrew, D. W., and Remington, S. J. (1998) Glycerol kinase from *Escherichia coli* and an Ala65 toThr mutant−The crystal structures reveal conformational changes with implications for allosteric regulation, *Structure 6*, 1407−1418.
25. Pawlyk, A. C., and Pettigrew, D. W. (2002) Transplanting allosteric control of enzyme activity by protein-protein interactions: Coupling a regulatory site to the conserved catalytic core, *Proc. Natl. Acad. Sci. U.S.A. 99*, 11115−11120.
26. Pawlyk, A. C., and Pettigrew, D. W. (2001) Subcloning, expression, purification, and characterization of *Haemophilus influenzae* glycerol kinase, *Protein Expr. Purif. 22*, 52−59.
27. Luque, I., and Freire, E. (2000) Structural stability of binding sites: Consequences for binding affinity and allosteric effects, *Proteins: Struct., Funct., Genet. 4*, 63−71.
28. Yu, P., and Pettigrew, D. W. (2003) Linkage between fructose 1,6-bisphosphate binding and the dimer-tetramer equilibrium of *Escherichia coli* glycerol kinase: Critical behavior arising from change of ligand stoichiometry, *Biochemistry 42*, 4243−4252.
29. Lakowicz, J. R. (1999) *Principles of fluorescence spectroscopy*, 2nd ed., Kluwer Academic, New York.
30. Pettigrew, D. W., Meadow, N. D., Roseman, S., and Remington, S. J. (1998) Cation-promoted association of *Escherichia coli* phosphocarrier protein IIA^{Glc} with regulatory target protein glycerol kinase: Substitutions of a zinc(II) ligand and implications for inducer exclusion, *Biochemistry 37*, 4875−4883.
31. Holtman, C. K., Pawlyk, A. C., Meadow, N. D., Roseman, S. R., and Pettigrew, D. W. (2001) IIA^{Glc} allosteric control of *Escherichia coli* glycerol kinase: Binding site cooperative transitions and cation promoted association by zinc(II), *Biochemistry 40*, 14302−14308.
32. Rusinova, E., Tretyachenko-Ladokhina, V., Vele, O. E., Senear, D. F., and Ross, J. B. A. (2002) Alexa and Oregon Green dyes as fluorescence anisotropy probes for measuring protein-protein and protein-nucleic acid interactions, *Anal. Biochem. 308*, 18−25.
33. Voss, E. W., Jr., Croney, J. C., and Jameson, D. M. (2002) Discrete bathochromic shifts exhibited by fluorescein ligand bound to rabbit polyclonal anti-fluorescein Fab fragments, *J. Protein Chem. 21*, 231−241.
34. Garcia, de la Torre, J., Huertas, M. L., and Carrasco, B. (2000) Calculation of hydrodynamic properities of globular proteins from their atomic-level structure, *Biophys. J. 78*, 719−730.
35. Ormo, M., Bystrom, C. E., and Remington, S. J. (1998) Crystal structure of a complex of *Escherichia coli* glycerol kinase and an allosteric effector fructose 1,6-bisphosphate, *Biochemistry 37*, 16565−16572.
36. Orte, A., Crovetto, L., Talavera, E. M., Boens, N., and Alvarez-Pez, J. M. (2005) Absorption and emission study of 2′,7′-difluorofluorescein and its excited state buffer-mediated proton exchange reactions, *J. Phys. Chem. A 109*, 734−747.
37. Bialik, C. N., Wolf, B., Rachofsky, E. L., Ross, J. B. A., and Laws, W. R. (1998) Dynamics of biomolecules: Assignment of local motions by fluorescence anisotropy decay, *Biophys. J. 75*, 2564−2573.
38. Ludescher, R. D., Peting, L., Hudson, S., and Hudson, B. (1987) Time-resolved fluorescence anisotropy for systems with lifetime and dynamic heterogeneity, *Biophys. Chem. 28*, 59−75.
39. Feinstein, E., Deikus, G., Rusinova, E., Rachofsky, E. L., Ross, J. B. A., and Laws, W. R. (2003) Constrained analysis of fluorescence anisotropy decay: Application to experimental protein dynamics, *Biophys. J. 84*, 599−611.
40. Lipari, G., and Szabo, A. (1980) Effect of librational motion on fluorescence depolarization and nuclear magnetic resonance relaxation in macromolecules and membranes, *Biophys. J. 30*, 489−506.
41. Vergani, B., Kintrup, M., Hillen, W., Lami, H., Piemont, E., Bombarda, E., Alberti, P., Doglia, S. M., and Chabbert, M. (2000) Backbone dynamics of Tet repressor α8α9 loop, *Biochemistry 39*, 2759−2768.
42. Schroder, G. F., Alexiev, U., and Grubmuller, H. (2005) Simulation of fluorescence anisotropy experiments: Probing protein dynamics, *Biophys. J. 89*, 3757−3770.
43. Guex, N., and Peitsch, M. C. (1997) Swiss-Model and the Swiss-Pdbviewer−An environment for comparative protein modeling, *Electrophoresis 18*, 2714−2723.

BI7010948